SYNTHESIS, CHARACTERIZATION AND PROCESSING OF NEW MATERIALS FOR INNOVATIVE APPLICATIONS
Jan-Mar 2024, VOL. 1, ISSUE 1, pp. 18-28
https://doi.org/10.61577/scpnmia.2024.100005

RESEAPRO JOURNALS

ORIGINAL ARTICLE

OPEN ACCESS

Activation of carbonized biomass materials as potential agents prepared for methylene blue adsorption

Etong Inyang Daniel[1], John Godwin[2], Nasir Abdus-Salam[3] and Mamman Ibrahim Alkali[4]

[1]Department of Chemical and Biochemical Science, Federal Polytechnic, Nigeria
[2]Department of Chemistry, Kogi State College of Education (technical), Kabba, Kogi State, Nigeria
[3]Department of Chemistry, University of Ilorin, Nigeria
[4]Department of Chemistry, Borno State University, Nigeria

ABSTRACT

Piliostigma thonningii (PSH), *Parquetina nigrescens* (PNS), and *Hildegardia barteri* (HB) activated carbon were prepared as adsorbents for methylene blue (MB) dye removal from aqueous solutions. The activation of raw materials with orthophosphoric acid (H_3PO_4) leads to carbons with high adsorption capacities. The biomasses were carbonized at 400 °C, 500 °C, and 600 °C, and the highest percentage yields were achieved at 400 °C. The biomasses were characterized using scanning electron microscope (SEM), energy dispersive X-ray (EDX), Fourier transform infrared (FTIR), and carbon, hydrogen, and nitrogen (CHN). They were used for batch adsorption of MB dye from aqueous solutions. Effects of initial concentration, contact time, pH, adsorbent dosage, and temperature were studied to determine the optimal condition of the activated carbon (AcC) adsorbents. The adsorption capacities of PSH, PNS, and HB were 55.25, 20.16, and 19.27 mg/g of MB, respectively. The negative value of ΔH of adsorption for PSH (-0.065 KJ/mol) shows that the adsorption was exothermic, while the positive value of ΔH for HB (+0.017 KJ/mol) and PNS (+0.128 KJ/mol) indicates that the adsorption of MB was endothermic. The positive values of ΔS (7.30 J/mol/K for PSH, 9.77 J/mol/K for HB, and 11 J/mol/K for PNS) revealed randomness of the adsorption processes at the sorbent-sorbate interfaces. Langmuir fitted better as the R^2 values were all close to unity, while the kinetics studies followed the Pseudo-Second Order for all the adsorbents. The result demonstrated that the AcC sets from the three biomasses have the potential to be employed as low-cost adsorbents.

KEYWORDS

Biomass; Methylene blue; Adsorption; Activated carbon; PSH-PNS-HB

ARTICLE HISTORY

Received 26 February 2024;
Revised 18 March 2024;
Accepted 25 March 2024

Introduction

The physical environment is facing the worst pollution in human history, with man being the pollution agent. The rise in industrial and domestic activities is instrumental in releasing pollutants into the water bodies, which directly affect humans, resulting in diverse health problems. Much research has been directed at solving environmental challenges, but no chemical agent has successfully solved the pollution menace, as little has been achieved yet. The application of inorganic materials has done appreciably well, but it also comes with the high cost of synthesis in terms of chemical acquisition and procedures. Consequently, green synthesis using biomass adsorbents is a better option for pollutant removal from the environment. Activated carbon (AcC), popularly applied in wastewater treatment in a variety of research works, can be prepared in different ways. It is a carbon prepared with increased surface area and many small-sized pores for adsorption purposes, and a small gram is 500 m^2. A high surface area is appropriate for useful application in adsorption, but activation using chemical methods increases the affinity of materials in adsorption. The adsorption property and efficiency of an adsorbent such as AcC is determined mainly by the type of method and starting in the preparation process.

In an adsorption study, jatropha husk, the agricultural solid waste generated by the bio-diesel industry, was used as a starting material for the production of AcC by Namasivayam et al. [1]. The efficiency of removing some pollutants, such as dyematerials from wastewater, was investigated. The findings suggest that jatropha husk AcC adsorbent was used to eliminate harmful heavy metal ions and other organic and inorganic contaminants. Studies by Bernard et al. examined the removal of some heavy metal ions (Pb, Fe, Cu, and Zn) from wastewater on AcC prepared from the coconut shell [2]. Batch experiments were performed and showed that the adsorption rate depended on factors like time, adsorbent mass, pH, and stirring speed. The removal of Cd^{2+} by sugarcane bagasse-based AcC using factorial design was investigated by Musa et al. [3], and the result was positive. Sethu et al. investigated the thermodynamic adsorption of Cu^{2+} ions from waste water using neem-leaf-based biosorbents and concluded that the optimum adsorption potential of neem leaf powder was 500 ppm with a value of 446.5 mg/g [4]. The results showed that the adsorption mechanism occurred naturally, showing that the adsorbent is a favorable biosorbent for extracting Cu^{2+} ions from aqueous solution. Similarly, Mohammed and Edward used cotton stalks as a source of AcC for the removal of some metal ions from the solution [5]. It was discovered that the AcC produced showed potential for adsorption of heavy metals in the batch equilibrium studies from both single and multi-component aqueous phases. The studies revealed that there is a high negative charge of AcC surface above pH 5.5. The studies revealed that adsorption was mainly by electrostatic

***Correspondence:** Dr. John Godwin, Department of chemistry, Kogi State College of Education (technical), Kabba, Kogi State, Nigeria, e-mail: godwinjohn1380@gmail.com

RESEAPRO JOURNALS

interaction between the negatively charged surface of the carbon adsorbent and the positively charged metal ions in the solution. Nevertheless, removal of the metal ions, in some cases, occurred at lower pH. Elaigwu et al. analyzed the adsorption of Pb^{2+} by AcC prepared from cow dung under different conditions [6]. The adsorption studies showed that the process was fast, stable, and took less than 100 minutes to attain equilibrium. In another research, the ability of *Phanerochaete crysosporium* to extract Cr ions from aqueous solution was investigated by Marandi [7]. The optimum pH for biosorption of Cr (VI) was 2 at a steady temperature of 25 °C. Similarly, Adebayo et al. studied the capacity of some prepared samples of AcC made from Jatropha curcas stem, root, and seed coat and concluded that the adsorbent labeled as ACS, ACR, and ACC activated with H_3PO_4 have good adsorbing capacity for Pb ions [8]. The Pb(II) ions adsorption was found to be maximal at pH 8. The numerous adsorption studies above and more in literature have shown that AcC biomass has been applied in the adsorption of many inorganic substances but is limited to organic materials such as dyes. The ones that were used for the removal of some dye molecules revealed low efficiencies and capacities. This is what forms the basis and design of this research work.

The optimum adsorption performance of *Piliostigma thonningii* (PSH), *Hildegardia barteri* (HB), and *Parquetina nigrescens* (PNS) biomass in removal of methylene blue (MB), was investigated by optimizing adsorption parameters such as concentration, adsorbent dose, absorption time, pH and temperature, and subjecting the adsorption processes to isotherm, kinetic and thermodynamic studies.

Materials and Methods

Sample collection

The biomass samples used in this study include PSH, HB, and PNS. Fruit shells were collected from farms in the Offa local government area of Kwara state, Nigeria.

Preparation of biomass sample

The samples were cracked using a hammer, and the seeds embedded in white pulp were removed, leaving the shells that were needed. The shells were properly washed using de-ionized water. Dilute nitric acid (0.01M) was also used to wash the shells to further remove impurities and then rinsed several times with de-ionized water till the pH of the washed water was neutral. The washed shells were air-dried for 5 days under laboratory conditions, and they were later used to produce AcC by a process of carbonization followed by chemical activation. The carbonization process converts the organic materials to primary carbon, whereas the activation process removes the decomposed products deposited in the pores and makes the AcC more porous in nature.

Preparation of activated carbon

Carbonization and activation

A 400 g sample of PNS, HB, and PSH was carbonized in a pyrolizer under a continuous flow of nitrogen gas and at temperatures of 400, 500, and 600 °C for 60 minutes duration. The charred products were allowed to cool to room temperature, crushed using mortar and pestle, and stored in air-tight containers. A 150 g of carbonized sample was weighed and transferred into a beaker containing 150 mL 75% ortho-phosphoric acid (H_3PO_4), ratio 1:1. The impregnation was carried out at 60 °C in a hot air oven for 24 h to achieve well penetration of chemicals into the interior of the precursor. The activated sample was then cooled to room temperature, washed with de-ionized water to neutral pH, oven-dried, and stored for characterization. After cooling, each of the carbonized materials was weighed to determine the percentage yield per mass of the raw sample used [8].

Characterization of adsorbents

The phase composition of the samples was analysed using energy dispersive X-ray (EDX), while scanning electron microscope (SEM) was used to determine the surface morphology of the samples. A CHN analyser was used for AcC to determine carbon, hydrogen, and nitrogen content, and functional groups present in the structure of the samples were appraised by Fourier transform infrared (FTIR) spectroscopy.

Study of effects of adsorption parameters

The effect of initial concentration was studied by taking 25 ml of 5, 10, 25, 50, 100, 250 mg/L of MB prepared from stock solutions and agitated each with 0.1 g of the adsorbents separately at 30 °C for 5 h. Each mixture was filtered, and the filtrates were analyzed using a UV spectrometer [9]. The quantity adsorbed, q_e, was calculated using Equation 2. The adsorbate concentration that gave optimal adsorption was determined through a plot of q_e versus initial metal ion concentration and was used in subsequent adsorption processes.

The effect of mass dose was investigated by taking 25 mL of the MB solutions in different conical flasks and agitating with 0.1, 0.5, 1.0, 1.5, and 2.0 g of the biomass adsorbent at 30°C. These experimental procedures were carried out in duplicate, and the mixtures were agitated on a mechanical shaker for 2 h, filtered, and the filtrates were analyzed for MB using a UV-Spectrometer. The quantity adsorbed, q_e, was calculated using Equation 2.

The effect of time was studied by taking 0.1 g of biomass adsorbent separately and agitating in different conical flasks with 25 mL of the optimum concentrations obtained for MB solutions for different time intervals of 5, 10, 15, 30, 45, 60, 90, 120, 180, 240 and 300 minutes. These experimental arrangements were carried out in duplicates. The solutions were filtered, residual metal ion concentrations were determined using a UV visible spectrophotometer, and the q_e was calculated using equation 2 [10].

The effect of temperature was carried out by varying the temperature starting from 30, 40, 50, 60 to 70 °C. A 25 mL of the optimum concentration obtained for MB was contacted with the optimum adsorbent dose in a 100 mL conical flask. The procedure was carried out in duplicates, and the mixtures were agitated on the shaker for the optimal time, filtered, and the filtrates were analyzed for MB. The q_e and efficiency of adsorption, in percentage, by the various adsorbents were calculated by using equations 2 [9,11].

The effect of pH on MB adsorption was carried out over a pH range of 2 to 8. A 25 ml of the optimum concentration of MB was agitated with the optimal dose of biomass adsorbent in different conical flasks; the solutions were filtered after

https://doi.org/10.61577/scpnmia.2024.100005

adsorption, and the filtrates were analyzed for MB using a UV-Spectrometer. The qe and efficiency removal in percentage were calculated by using equation 2 [9].

Determination of adsorption capacity

The amount of metal ions adsorbed, q_e (mg/g), by biomass adsorbents was calculated using equation 1, while the efficiency of adsorption in percentage (% R_{em}), which is metal ion removed from aqueous solutions by the adsorbents was estimated by equation 2 [12]:

$$q_e = \frac{C_0 - C_e}{M} \times V \quad (1)$$

$$\%R_{em} = \frac{C_0 - C_e}{C_0} \times 100 \quad (2)$$

Where C_o and C_e are the initial and equilibrium concentration of metal ions in solution at any time (t) in (mg/L), V (L) is the total volume of the metal ions, and M is the mass (g) of adsorbent used.

Isotherm of adsorption

The Langmuir, Freundlich, and intraparticle diffusion adsorption parameters were used to study the adsorption nature of this study. The Langmuir adsorption isotherm describes the homogenous adsorption layer between the sorbate-sorbent particles. The linear form of the Langmuir is represented in equation 3.

$$\frac{1}{q_e} = \frac{1}{q_m} + \frac{1}{q_m K_L C_e} \quad (3)$$

Where q_m (mg/g) is maximum monolayer coverage capacity, and K_L is Langmuir isotherm constant (L/mg). The slope and intercept of the Langmuir plot were determined from the values of K_L and q_m. In terms of the equilibrium parameter, R_L is an essential characteristic of the Langmuir isotherm determined using equation 4.

$$R_L = \frac{1}{1 + K_L C_o} \quad (4)$$

Where: R_L value indicates the adsorption nature, which shows whether adsorption is unfavorable (R_L>1), linear (R_L = 1), favorable (0 < R_L < 1), or irreversible (R_L = 0).

The Freundlich isotherm shown in linear equation 5 describes heterogeneous adsorption on the surface of adsorbents [10, 13].

$$Log q_e = Log K_f + 1/n log C_e \quad (5)$$

Where K_f is Freundlich isotherm constant (mg/g), n is adsorption intensity, while 1/n is a function of the strength of adsorption [14]. If n = 1, the partition between the two phases is independent of the concentration. Where the value of 1/n is <1, normal adsorption is indicated, while 1/n >1 indicates cooperative adsorption.

The Temkin isotherm assumes that the adsorption heat of all molecules in the layer will decrease linearly rather than logarithmic with coverage. It is defined by a uniform distribution of binding energies, which was determined by plotting the q_e against lnC_e, where the slope and intercept were obtained. The linear equation 6 is used to determine the Temkin parameters [15].

$$q_e = \frac{RT}{b_T} ln A_T + \frac{RT}{b_T} ln C_e \quad (6)$$

$$B = \frac{RT}{b_T} \quad (7)$$

Where A_T is Temkin isotherm equilibrium binding constant (L/g), b_T is Temkin isotherm constant, R is universal gas constant (8.314 Jmol^{-1}K^{-1}), T is Temperature at 298K (25 °C), and B is Constant related to the heat of sorption (Jmol^{-1}).

Adsorption kinetics

A first-order rate equation (Eq. 8) is based on adsorption capability [16].

$$\ln(q_e - q_t) = \ln q_e - k_1 t \quad (8)$$

Where qt (mg/g) is the adsorption capacities at time, t (min), while k^1 (min^{-1}) is the pseudo-first-order rate constant for the kinetic model. A straight-line curve obtained from linear plots of $ln(q_e\text{-}q_t)$ against twith regression coefficient, R^2 value close to unity, determines the fitness of adsorption data for the kinetic model.

The pseudo-second-order kinetics model is given in equation 9.

$$\frac{t}{q_t} = \frac{1}{k_2 q_e^2} + \frac{1}{q_e} t \quad (9)$$

Where K^2 is the pseudo second order rate constant (g mg^{-1} min^{-1}). This is a straight-line graph obtained from a linear plot of t/qt against t.

The intra-particle diffusion model describes mass transfer in an amorphous and homogenous process. In several phases, adsorbate movement from the aqueous phase to the surface of the adsorbent pores takes place. The intra-particle diffusion in equation 10 was used to estimate the various constants.

$$q_t = K_{id} t^{1/2} + I \quad (10)$$

Where Kid is the rate constant of intra-particle diffusion (mg/g min$^{-½}$) and I is the intercept. The value of I provides an indication of the thickness of the boundary layer [17]. The intra-particle diffusion model is indicated by a plot of q_t versus t^{½}, where the values of K_{id} were calculated. A straight-line plot of qt versus t^{½} shows that the sorption mechanism is controlled by an intraparticle diffusion process.

Adsorption thermodynamic studies

The adsorption thermodynamic study of MB dye onto PNS, PSH, and HB AcC was carried out by evaluating the enthalpy change (ΔH), the free energy change (ΔG), and the entropy change (ΔS). The nature and spontaneity of the adsorption process are determined by values of ΔH and ΔS. Adsorption is endothermic and exothermic, with positive and negative values of ΔH, respectively, and negative values of ΔG indicates the feasible adsorption process. The values of ΔH and ΔS were estimated from equation 11, while ΔG was determined from equations 13 and 14, respectively,

$$InK_{ad} = \frac{\Delta S}{R} - \frac{\Delta H}{RT} \quad (11)$$

$$K_{ad} = \frac{q_e}{C_e} \quad (12)$$

$$\Delta G = -RTInK_{ad} \quad (13)$$

$$Ink_2 = InA - \frac{E_a}{RT} \quad (14)$$

where K_{ad} is the adsorption coefficient, R is the gas constant, and k_2 is the rate constant. The ΔH was estimated from the plot of InK_{ad} verses *1/T*.

Results and Discussion

Percentage yield from carbonization process

The effects of charring temperature and time, which seriously influenced the surface area yield of adsorbent and bulk density, were studied. Percentage yield is an important parameter that

https://doi.org/10.61577/scpnmia.2024.100005

RESEAPRO JOURNALS

is used to ascertain the rate of the carbonization process. Results for the percentage yield of char during various conditions are shown in Table 1. It was observed that there is a direct relationship between charring temperature and percentage yield. The highest percentage yield was attained at 400 °C and 60 min for all three samples. This is because increasing time and/or increasing temperature of carbonization resulted in more volatile components being lost and hence decreasing percentage yield [18]. The highest observable percentage yield for PSH, HB, and PNS was 41.61, 40.09 and 29.40 %, respectively, at 400°C for 60 min., while the least was at 600 °C for 60 min, and the yield was 17.20, 29.40, and 28.70% for HB, PSH, and PNS respectively. The negative effect of carbonization temperature and time was most felt at the highest experimental temperature of 600 °C [19].

Characteristic of adsorbents

Table 1. Carbonization time and temperature for HB, PSH, and PNS AcC.

Sample Code	HBa	HBb	HBc	PSHa	PSHb	PSHc	PNSa	PNSb	PNSc
Charring Temperature(°C)	400	500	600	400	500	600	400	500	600
Charring Time (min)	60	60	60	60	60	60	60	60	60
%Yield	40.09	18.10	17.20	41.61	31.44	29.40	29.40	30.60	28.70

The physico-chemical characteristic of the adsorbent with carbonization time of 60 min and 400 °C is presented in Table 2. The moisture content was approximately the same for the three biomasses. The moisture content ranges from 0.22 ± 0.03 - 0.44 ± 0.01%, which was lower than banana empty fruit bunch (BEFB), 5.21 ± 0.16% [20]. The % ash is higher in PNS (4.20 + 0.03%) than PSH (3.40 ± 0.02%), and HB (2.80 ± 0.02%), but all were lower than banana empty fruit bunch (15.73 + 1.66%), [20]. The ash content is a reflection of the amount of inorganic substituent present, and the higher the value, the higher the value of inorganic constituents. The ash content was within the range of most AcC from agricultural products (0.2 - 13.4%) [21]. The % carbon yield was higher for PSH (41. 61 + 0.04) than HB (40.09 + 0.04), while PNS was the least (29.40 ± 0.03).

This study shows that PNS has a higher bulk density of 0.636 + 0.01 g/mL than KOH-treated DRFP (0.46g/ml), while HB was found to be 0.450 + 0.01g/ml compared to KOH-treated DRFP [20]. The bulk density shows the precursor's fiber quality. The lower the weight, the better its level of regeneration after use [22]. A sample's iodine number is expressed as the proportion of iodine adsorbed per gram of the sample. The iodine amount of HB (950 + 25 mg/g) was found to be higher than that of PNS (900 + 20 mg/g) and PSH (850 + 10 mg / g). This may be because HB is more porous than both of them. The activation process increases the surface area and porosity as well as lowers the surface acidity of the AcC, which gives rise to low pH values of 4.4 and 5.7 observed for HB and PSH, respectively.

Table 2. Physico-chemical characteristic of adsorbent (% wt) dry basis.

Parameter	PSH AcC	PNS AcC	HB AcC
Moisture (%)	0.33±0.01	0.44±0.01	0.22±0.03
Ash (%)	3.40±0.02	4.20±0.03	2.80±0.02
Carbon yield (%)	41.61±0.04	29.40±0.03	40.09±0.04
Bulk Density (g/ml)	0.635±0.01	0.636±0.01	0.450±0.02
Iodine Number (mg/g)	850.0±10	900.0±20	950.0±25
pH	5.70	6.50	4.40

pH_{pzc} of adsorbent

The pH_{pzc} of PNS, PSH, and AcC were determined by the pH drift method, which gave 7.5 pH_{pzc} for HB, 4.1 for PSH, and 4.9 for PNS. The value for HB was in close agreement with Nassar and Rings red (7.5 +0.5) [23]. Positive pH values of pH_{pzc}, favor the adsorption of negatively charged species, while negatively charged surfaces favor the adsorption of positively charged species. The pHpzc for PSH and PNS is in the acidic region, while HB is in the basic region. The graphs of the pH_{pzc} are shown in the Figures. 1 (a)-(c).

CHN analysis of PNS, PSH, and HB AcC adsorbents

The result of the CHN analysis is presented in Table 3, and it shows that HB has the highest percentage of carbon (72.27%) and PNS the least (68.42%). PNS has the highest percentage of hydrogen and nitrogen, i.e., 3.71 and 3.42%, respectively. HB has the least value of hydrogen and nitrogen, i.e., 2.82% and 1.20%, respectively. The value for carbon was within the range reported for most agricultural materials (41.23 – 84.50%), hydrogen was below the range (4.63 - 6.26%), while nitrogen was within the range (0.7 – 4.10%) [21]. The carbon, hydrogen, and nitrogen content of PNS was higher than that of mango seed (carbon 52.31%, hydrogen 3.38%, and nitrogen 1.02%), while PSH and HB were higher in carbon and nitrogen but lower in hydrogen than mango seed [22].

https://doi.org/10.61577/scpnmia.2024.100005

RESEAPRO JOURNALS

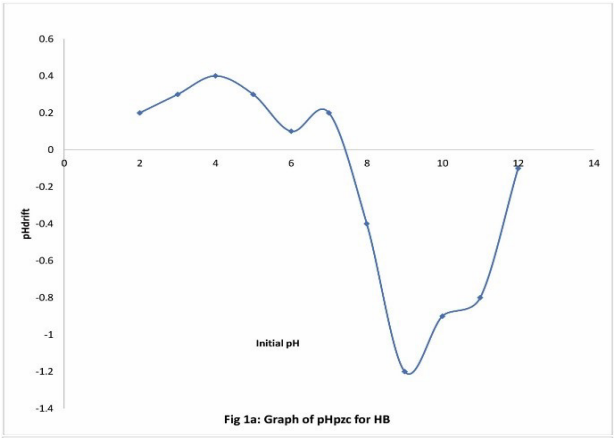

Fig 1a: Graph of pHpzc for HB

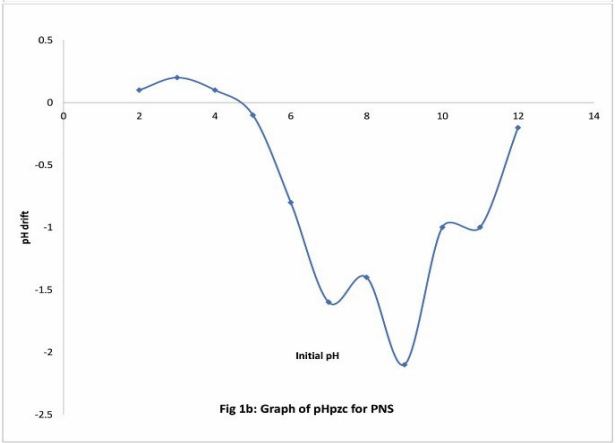

Fig 1b: Graph of pHpzc for PNS

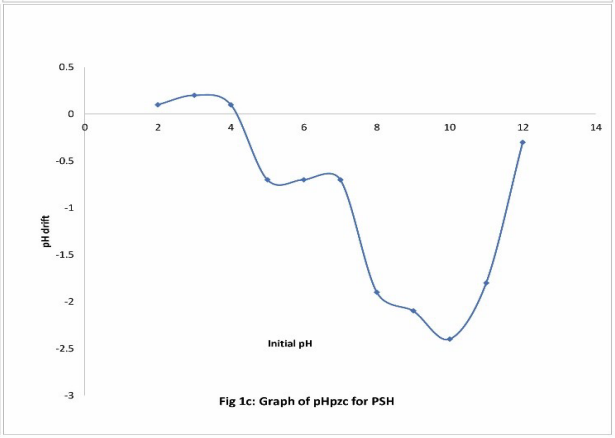

Fig 1c: Graph of pHpzc for PSH

Figure 1(a). Graph of pHpzc for HB. (b). Graph of pHpzc for PNS. And (c). Graph of pHpzc for PSH.

Table 3. CHN Analysis.

Biomass	% C	% H	% N
PNS	68.42	3.71	3.42
PSH	69.42	3.34	2.06
HB	72.27	2.82	1.20

SEM analysis of PNS, PSH, and HB AcC adsorbents

The SEM spectra results obtained from the analysis at different magnifications (1,000x and 50,000x) are presented in Figures 2 (a)-(c). The sample particles showed a dense, irregular leaf-like shape that tends to agglomerate; smaller and homogenous particles were also found in PSH 1000x magnification. The surface of the PNS particles showed larger pores (high porosity). These pores will be readily available for composite formation with other adsorbents or adsorption processes, making the sample have prospects in practical application to the adsorption process. The 50,000x magnification of the samples showed agglomeration in sheet-like structures comparable to treated and untreated BEFB [20].

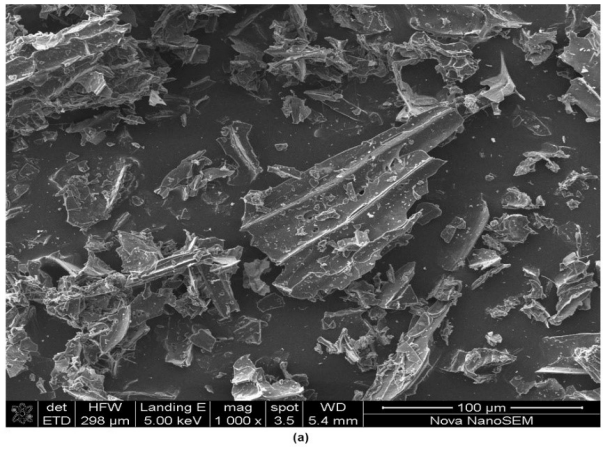

(a)

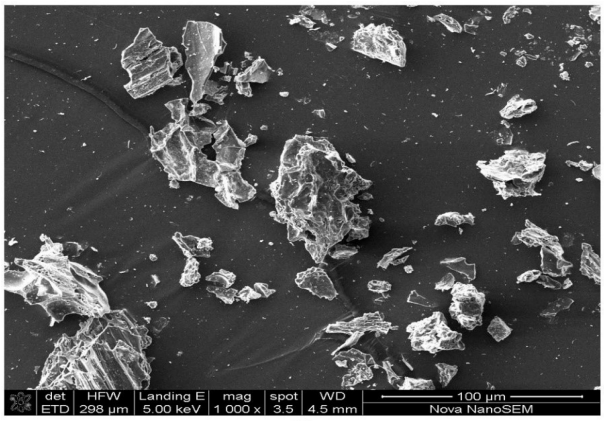

(b)

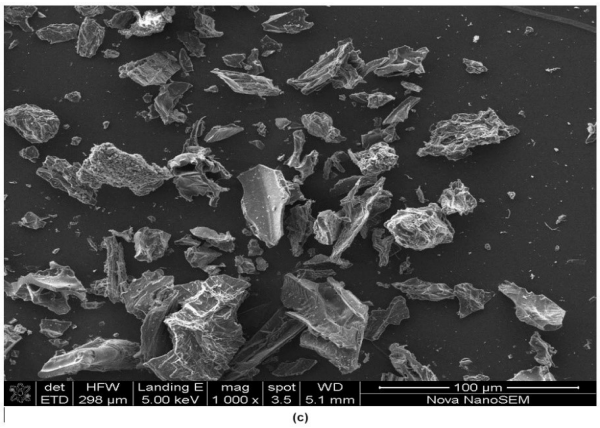

(c)

Figure 2(a)-(c). 1,000X magnifications for HB, PNS, and PSH AcC.

EDX analysis of PNS, PSH, and HB AcC adsorbents

The EDX analysis was carried out using Perkin Elmer C624 to determine the element's composition of the sample as reported in Table 4 and Figures 3 (a)-(c). Carbon was the predominant

https://doi.org/10.61577/scpnmia.2024.100005

element in the samples with 79.20% for HB, 79.06% for PSH and 76.39% for PNS. Nitrogen was absent in PSH and HB, while it was 5.52% for PNS. Oxygen was highest in PSH, with a value of 20.84%, followed by HB at 20.23%. The insignificant percentage of phosphorus in HB and PSH were found as impurities. The EDX results for carbon were slightly higher than that of CHN but practically close. The EDX values for carbon ranges from 76.39–79.20%, while the CHN ranges from 68.42–72.27%. The values for carbon were within the range reported for most agricultural materials (41.23–84.50) [21]. The higher the carbon content, the more desirable the material is as a precursor for AcC preparation.

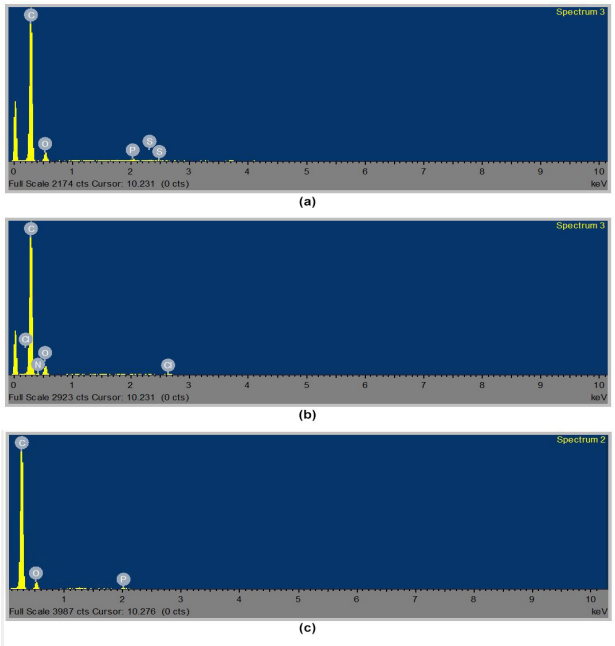

Figure 3(a). EDX graph for HB AcC. (b). PNS AcC. and (c). PSH AcC.

Table 3. EDX Analysis for activated carbon.

Biomass	% C	% O	% N	% Cl	% S	% P
PSH	79.06	20.84	-	-	-	0.1
PNS	76.39	17.93	5.52	0.16	-	-
HB	79.20	20.23	-	-	0.22	0.35

FTIR analysis of PNS, PSH, and HB AcC adsorbents

The spectra were recorded over the range of 4000 - 500 cm-1, as shown in Figures 4(a)-(c). The various absorption bands obtained were utilized in the characterization of the adsorbents using reported values [24]. The broadband 3000 - 4000 cm-1 centered at 3563.06 cm-1 and 3160.95 cm-1 can be assigned to O-H stretching and bending vibrations arising from surface hydroxyl groups on adsorbent particles and water. Two weak absorption bands occurring at 2771.50 cm-1 and 2055.94 cm-1 in the spectrum correspond to H-O-H bending and stretching vibration mode [25, 26]. The spectra of HB showed a prominent peak at 2347.23 cm-1 that is attributed to C C stretching vibration. Peaks were also observed at 1701.32 and 1593.67 cm-1, depicting C = O stretching and conjugated C = C [22]. The spectrum of PNH AcC was recorded over a range of 4000 - 500 cm-1, and a peak was observed at 2920.32 cm-1, which is attributed to the C-H asymmetric stretching vibration of CH2. Other peaks were seen at 2350.40 cm^{-1}, 1704.49, 1448.02, and 874.93/811.61/748.28 cm^{-1} depicting C≡C stretching vibration, C=O stretching, methyl C-H asymmetric/ symmetric bend, and C-H bending (out of plane) vibration respectively. Fig. 4c shows the typical spectrum of PNS AcC as recorded over the range of 4000 - 500 cm-1. It shows a prominent peak at 2926.65 cm-1 that is attributed to the C-H asymmetric stretching vibration of CH2. A strong absorption was noticed at 2350.40, 1704.49, 1606.33, and 874.93/783.11 cm-1, which indicates C≡C stretching vibration, C=O stretching, conjugated C = C and C-H bending (out of plane) vibration, respectively [27].

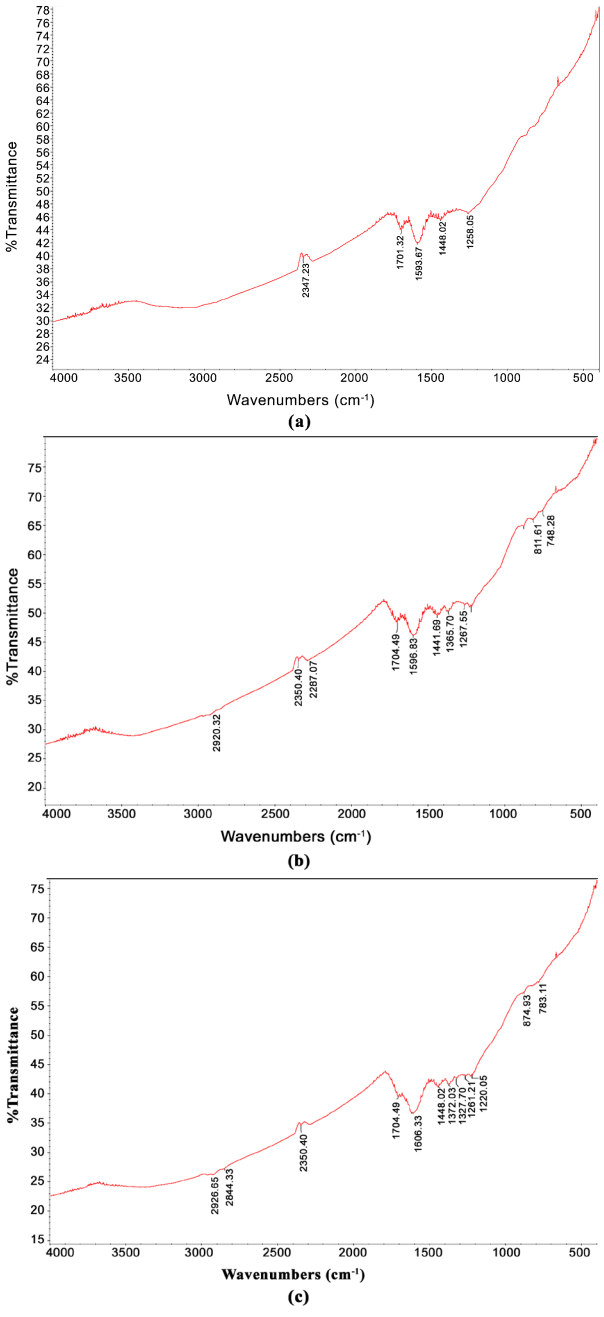

Figure 4(a). FTIR spectrum for HB AcC (b). PSH AcC. and (c). PNS AcC.

https://doi.org/10.61577/scpnmia.2024.100005

Batch adsorption experiment

Initial concentration effect of adsorption of MB

The results of the effect of initial MB dye concentration on PNS, PSH, and HB are plotted in Figure 5a. Based on the findings, the amount adsorbed also increased proportionally when the initial concentration was increased. From the initial concentration, the percentage of removal of MB increased from 10 to 50 ppm and became constant from 50 to 400 ppm. The fact that the initial MB concentration provides an enormous driving force that overcomes mass transfer resistance between the solid-aqueous interface was due to enormous vacant sites on the surface of the adsorbent. This is a result of a fixed number of active sites on the surface of the adsorbent at a constant dose. As the initial MB concentration was increased, the adsorbent's available active sites decreased, and this made the removal of MB dependent on the initial concentration [28]. Also, as the amount of MB molecules per unit volume of solution increases, the ratio of the amount of MB at the surface of the available adsorption sites also increases, and more MB molecules in solution can be adsorbed by the adsorbent which results in the increase of the equilibrium adsorption capacity [28].

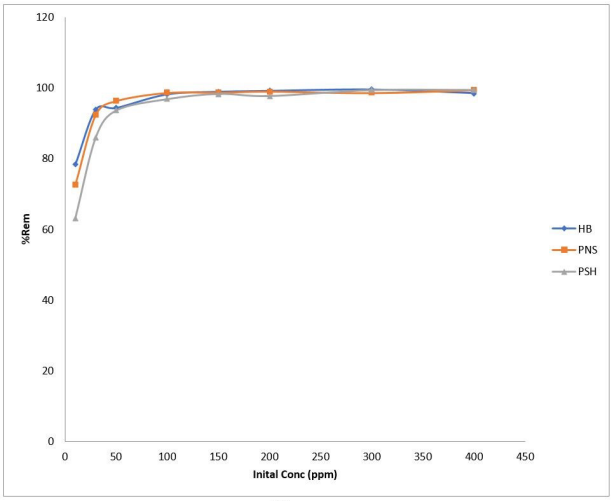

(a)

Figure 5(a). Effect of concentration on adsorption capacity of MB onto HB, PNS & PSH AcC.

Contact time effect on adsorption of MB

The plot of the effect of agitation time on the adsorption of MB on HB, PSH, and PNS AcC are depicted in Figure 5b. A fast phase at the beginning (0 - 90 min) was observed, where adsorption was rapid, which led to the equilibrium uptake of MB by 5.82 mg/g HB (97.87%), 5.83mg/g PNS (97.18%) and 5.74 mg/g PSH (95.68%). The second phase is a slow phase that occurs after the optimum adsorption from 120 to 300 Mins, where the adsorption capacity drops. The MB adsorption step was rapid, which is caused by the adsorption of MB onto the surface of HB, PNS, and PSH AcC adsorbent, while a slow-step diffusion-controlled phase followed the external adsorption step. A similar observation was earlier reported by Abdus-Salam and Buhari [22]. The optimum time for adsorption of this dye onto HB, PSH, and PNS was 90 min.

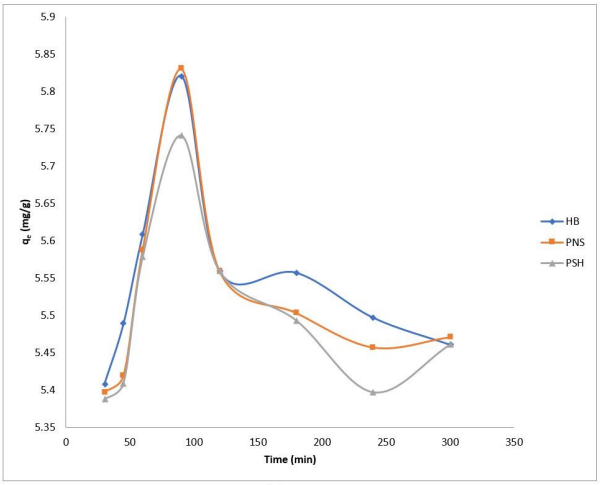

(b)

Figure 5(b). Effect of time on adsorption capacity of MB onto HB, PNS & PSH AcC.

Adsorbent mass effect on adsorption of MB

Figure 5c. shows that as the adsorbent dose was increased, the quantity of MB adsorbed by PSH, HB, and PNS decreased. This may have been due to the high adsorbent concentration resulting in adsorbent particle interaction that contributed to a reduction of the adsorbent's active surface due to overlap [29]. The decrease in the adsorbent quantity as the adsorbent dosage increases is attributable to the fact that raising the adsorbent mass decreases the unsaturation of the sites of adsorption. The number of active locations per unit mass has, therefore, decreased, resulting in comparatively less adsorption [30].

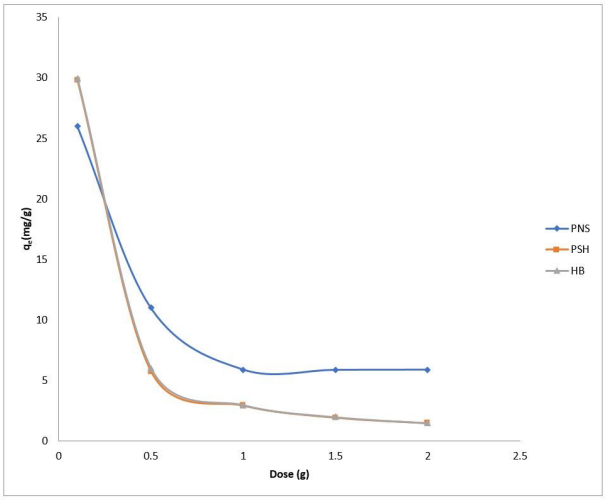

(c)

Figure 5(c). Effect of adsorbent dosage on adsorption capacity of MB onto HB, PNS & PSH AcC.

pH effect on adsorption of MB

In Figure 5d, it can be observed that the adsorption quantity and percentage removal of the dye by PSH, PNS, and HB AcC increase with an increase in pH [31]. At lower pH between 2-4, the adsorption of MB dye from the aqueous solution by the three adsorbents was very slow. This may be due to the hydrolysis of the adsorbents in water, which creates a positively

https://doi.org/10.61577/scpnmia.2024.100005

RESEAPRO JOURNALS

charged site, leading to the competition of H^+ ions with the cationic molecules of the dye, causing a decrease in the amount of dye absorbed [32]. The adsorption then increased more slowly from pH 5 to 8, which was almost constant. The maximum adsorption was achieved at pH 8. MB (cationic dye) bearing a positive charge and thus a basic dye showed maximum quantity adsorbed and percentage removal at a higher pH of 8. This is a result of electrostatic interaction between the OH^- group at higher pH on the surface of the adsorbent and the positive charge of the dye leading to better efficiency at higher pH, unlike what was observed at lower pH where the presence of H^+ competes (electrostatic repulsion) with the dye for active sites of the adsorbent (table 5) [31].

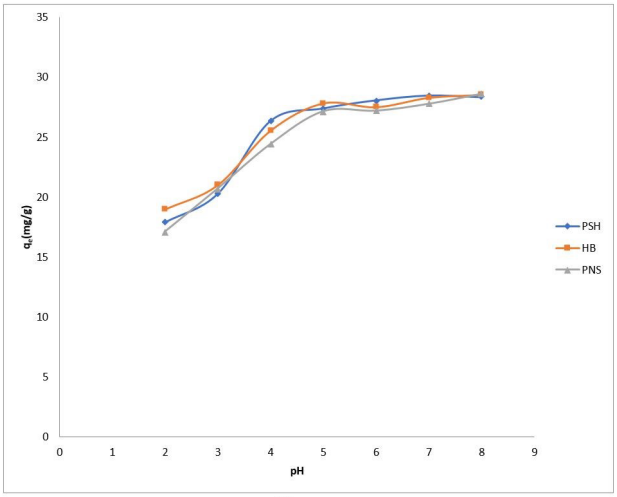

(d)

Figure 5(d). Effect of pH on adsorption capacity of MB onto HB, PNS & PSH AcC.

Table 5. Maximum adsorption capacity of different adsorbents for MB adsorption.

Adsorbents	Adsorbent capacity q_m(mg/g)	Reference
Poplar Sawdust	4.34	[33]
Brazil nut shells	7.81	[34]
Posidonia oceanic (L) fibres	5.56	[35]
Oyster shell	0.084	[36]
Short-neck clam shell	0.893	[36]
Natural jordaman Tripoli	16.6	[37]
Miswak leaves	200	[38]
Palm branches	14.30	[39]
HB	19.27	This work
PSH	55.25	This work
PNS	20.16	This work

Temperature effect on adsorption of MB

Figure 5e shows the influence of temperature change on the quantity adsorbed of MB removed from aqueous solution using the three adsorbents. It was observed from the results that the qe increased from 27.303 mg/g (91.245%) to 28.312 mg/g (94.373%), 27.403 mg/g (91.345%) to 28.122 mg/g (93.740%) and 27.503 mg/g (91.445%) to 28.169 mg/g (93.898%) onto HB, PNS and PSH AcC respectively when the temperature was increased from 30 °C to 50 °C. The optimum adsorption temperature was achieved at 50 °C for PNS, PSH, and HB adsorbents, and beyond this temperature, there was only little change in the qe of MB for all the adsorbents. The increase in quantity adsorbed may result from an increase in the diffusion rate of MB as a result of penetration of MB across the adsorbent membrane at higher temperatures [40]. The little change experienced after the optimum temperature is a result of the saturation of the active sites and sorbate-sorbent bond breakdown.

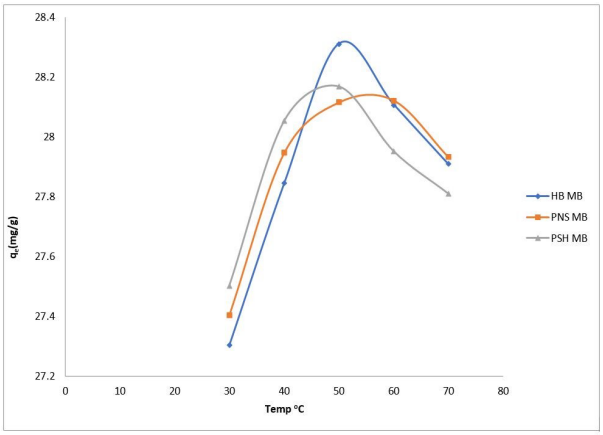

(e)

Figure 5(e). Effect of temperature on adsorption capacity of MB onto HB, PNS & PSH AcC.

Isotherm studies of MB adsorption

The equilibrium adsorption isotherm modeling of the adsorption of MB is presented in Table 6. The value of K_F measures the adsorption capacity of the adsorbent, while n determines the adsorbent surface heterogeneity and also indicates the degree of non-linearity between solutions. The K_F and n values are given in Table 6 to be 1.4676 mg/g and 1.4288 for PSH, 1.7894 mg/g and 1.8169 for PNS, and 2.6140 mg/g and 2.1173 for HB, respectively. The values of n are greater than one ($n > 1$), which indicates good adsorption processes for the three adsorbents. The K_F values show that HB has a higher ability to adsorb MB dye compared to PSH and PNS. The maximum binding energy, A_T are 3.0036, 1.1128, and 1.0191 L/mg for PSH, PNS, and HB, respectively. The values of the constant, b, are 4.9012, 4.8347, and 4.9447 $Jmol^{-1}$ for PSH, PNS, and HB, respectively, showing the heat of adsorption of MB on the three adsorbents. The correlation coefficient (R^2) is 0.8699, 0.8302, and 0.827 for PSH, PNS, and HB, respectively, showing that the adsorption of MB onto PSH, PNS, and HB fitted well with Temkin isotherm [22]. The Langmuir qm and K_L are 55.2486 mg/g and 0.006 L/mg for PSH, 20.1613 mg/g and 0.0850 L/mg for PNS, and 19.2678 mg/g and 0.1453 L/mg for HB. These q_m values are higher than those reported for similar adsorption studies of alizarin and fluorescein dyes on mango seeds with lower K_L values [22]. The correlation coefficient (R^2) is 0.9974, 0.9937, and 0.9718 for PSH, PNS, and

https://doi.org/10.61577/scpnmia.2024.100005

RESEAPRO JOURNALS

HB, respectively. In general, the results showed that the experimental data fitted well into the isotherms in the order of Langmuir > Freundlich > Temkin. The values of the factor R_L for PSH, PNS, and HB are 0.9434, 0.5405, and 0.4077, respectively, showing that the values are between 0.4 and 0.9, which revealed that the adsorption is favorable [41].

Table 6. Isotherm parameter for MB adsorption on PSH, PNS, and HB AcC adsorbents.

Isotherm model	Parameter	PSH AcC	PNS AcC	HB AcC
Freundlich Isotherm	K_F	1.4676	1.7894	2.6140
	N	1.4288	1.8169	2.1173
	R^2	0.9092	0.9482	0.9494
Temkin Isotherm	A_T (L/mg)	3.0036	1.1128	1.0191
	B ($Jmol^{-1}$)	4.9012	4.8347	4.9447
	R^2	0.8699	0.8302	0.827
Langmuir Isotherm	K_L (L/mg)	0.0060	0.0850	0.1453
	q_m (mg/g)	55.2486	20.1613	19.2678
	R_L	0.9434	0.5405	0.4077
	R^2	0.9974	0.9937	0.9718

Kinetic studies of MB adsorption

Kinetic analysis results for MB adsorption onto PSH, PNS and HB AcC is shown on Table 7. It was observed from the Table that the calculated q_e, cal values (5.4407 for PSH, 5.7937 for PNS and 5.814 for HB) are in close agreement with the experimental (q_e, exp) values for the three adsorbents unlike the pseudo - first order. This revealed that the adsorption of MB onto the three adsorbents followed a pseudo second order kinetic model. This is further confirmed by a very high correlation co-efficient value (R_2 of 0.9999 for PSH, 1 for both PNS and HB). The working of the pseudo second order for the adsorption of MB onto PSH, PNS and HB indicates that the concentration of MB and the adsorbents are involve in rate determining step [42]. The intra-particle rate constant in Table 7 shows that the K_{id} values are -0.0077 for PSH, -0.0024 for PNS and -0.0038 for HB. The result indicated that the plot was non-linear over the whole-time range and the curves does not pass through the origin showing that the intra-particle diffusion was not the only rate determining step, but may control adsorption rate [43]. The low values of K_{id} also indicated that intra-particle diffusion mechanism is not the predominant mechanism in the adsorption of MB onto the three adsorbents [44]. The pseudo-second order shows that the calculated quantity adorbed, qe,cal, and the experimental quantity adsorbed, qe,exp., in Table 7 are in close agreement unlike the pseudo-first order. The pseudo-second-order rate constant (k_2) and the adsorbed quantity of q_e,cal were obtained from the plot slope and intercept of t/qt vs. t and are shown in Table 7. It further shows that the adsorption of MB onto the adsorbents followed pseudo-second order kinetics.

Table 7. Kinetic data for MB adsorption on PSH, PNS, and HB AcC adsorbents.

Kinetic model	Parameter	PSH AcC	PNS AcC	HB AcC
Pseudo-First-Order	$k_1(min^{-1})$	-2.0×10^{-5}	0.0026	0.0073
	$q_{e\ cal}$(mg/g)	0.3046	0.0157	0.0078
	$q_{e\ exp}$(mg/g)	5.7410	5.8454	5.8441
	R^2	3.0×10^{-5}	0.0265	0.4861
Pseudo-Second-Order	$k_2(gmg^{-1}min^{-1})$	0.00	0.00	0.00
	$q_{e\ cal}$(mg/g)	5.4407	5.7937	5.814
	$q_{e\ exp}$(mg/g)	5.7410	5.8454	5.8441
	R^2	0.9999	1	1
Intra-particle-Diffusion	K_{id} (mg/ $gmin^{-0.5}$)	-0.0077	-0.0024	-0.0038
	C	5.5242	5.848	5.853
	R^2	0.1174	0.3705	0.6621

Thermodynamic studies of adsorption of MB

The negative values of ΔG indicate the degree of spontaneity of the adsorption of MB onto the surface of PSH, HB, and PNS, showing no external energy source. It can also be observed that the negative value of the ΔG increases from -2.21 to -2.57 KJmol, -2.94 to -3.33 KJ/mol, and - 3.20 to -3.64 KJ/mol for PSH, HB, and PNS respectively, reflecting more energetic favorable adsorption at a higher temperature. Generally, a value between 0 to -20 kJ/mol for ΔG is considered physical adsorption, such as electrostatic attraction. Values of ΔG in the range of -80 to -400 KJ/mol denote chemical adsorption [45]. Therefore, the adsorption of MB onto the three adsorbents is physical adsorption with a weak force of attraction between MB molecules and the three adsorbents. The negative value of ΔH for PSH (-0.065 KJ/mol) shows that the adsorption was exothermic in nature, while the positive value of ΔH for HB 0.017 KJ/mol and 0.128 KJ/mol for PNS indicated that the adsorption of MB onto the two adsorbents are endothermic in nature. The positive values of ΔS (7.30 J/mol/K for PSH, 9.77 J/mol/K for HB, and 11 J/mol/K for PNS) suggest that there is an increase in randomness at the sorbent-sorbate solution interface during the adsorption of MB onto the surface of PSH, HB and PNS adsorbent (table 8) [45].

https://doi.org/10.61577/scpnmia.2024.100005

Table 8. Thermodynamic parameters calculated for the adsorption of methylene MB onto PSH, HB, and PNS AcC adsorbents.

Adsorbent	T (K)	ΔG (KJ/mol)	ΔS (J/mol/K)	ΔH (KJ/mol)
PSH AcC	303	-2.21	+7.30	-0.065
	313	-2.35		
	323	-2.42		
	333	-2.49		
	343	-2.57		
HB AcC	303	-2.94	+9.77	+0.017
	313	-3.04		
	323	-3.14		
	333	-3.24		
	343	-3.33		
PNS AcC	303	-3.20	+11.00	+0.128
	313	-3.31		
	323	-3.42		
	333	-3.53		
	343	-3.64		

Conclusions

The adsorption of MB dye molecules on AcC from PSH, (HB), and (PNS) from aqueous solution was found to be more efficient compared to most commercially available adsorbents found in the literature. The adsorption of the dye molecules was pH dependent and temperature and fitted well into Langmuir isotherm, showing a monolayer and homogeneous adsorption process. The kinetic studies indicated that the adsorption process fitted well to the pseudo-second-order kinetic model, while the adsorption thermodynamics gave positive values for Δ H° and ΔS° showing the endothermic and random process at the adsorbent-aqueous interphase with negative ΔG° values showing that the process is spontaneous in nature. The value of activation energy also suggests that the adsorption of MB is physical adsorption, indicating that the adsorbent materials can be recovered and reusable.

Disclosure statement

No potential conflict of interest was reported by the authors.

References

1. Namasivayam C, Sangeetha D, Gunasekaran R. Removal of anions, heavy metals, organics and dyes from water by adsorption onto a new activated carbon from jatropha husk, an agro-industrial solid waste. Process Saf Environ Prot. 2007;85(2):181-184. https://doi.org/10.1205/psep05002
2. Bernard E, Jimoh A, Odigure J. Heavy metals removal from industrial wastewater by activated carbon prepared from coconut shell. Res J Chem Sci. 2013;3(8):3-9.
3. Mutah M, Akira K, Zaiton AM, Jafariah J, Razman SM, Eman IN. Production of sugarcane bagasse based activated carbon for $Cd2^{+}$ removal using factorial design. Int J Innov Technol Explor Eng. 2023;2(4):121-125.
4. Sethu V, Kua Y, Quek WS, Lim KV, Andresen J. Adsorption thermodynamics of Cu2+ ions from waste water using neem leaf base biosorbents. J Environ Res Develop. 2011;6(1):26-33.
5. El Zayat MA, Smith E. Removal of heavy metals by using activated carbon produced from cotton stalks. Can J Environ Constr Civ Eng. 2010;1(4):71-79.
6. Elaigwu SE, Usman LA, Awolola GV, Adebayo GB, Ajayi RM. Adsorption of Pb(II) from aqueous solution by activated carbon prepared from cow dung. Adv in Nat Appl Sci. 2009;3(3):442-446. http://dx.doi.org/10.3923/erj.2010.257.260
7. Marandi R. Biosorption of hexavalent chromium from aqueous solution by dead fungal biomass of *Phanerochaete crysosporium*: batch and fixed bed studies. Can J Chem Eng Technol. 2011;2(2):8-22.
8. Adebayo GB, Abdus-salam N, Elelu SA. Adsorption of Lead (II) ions by activated carbon prepared from different parts of *jatropha curcas* plant. Ilorin J Sci. 2014;1(1):28-49. https://doi.org/10.54908/iljs.2014.01.01.003
9. Abdus-Salam N, Itiola AD. Potential application of termite mound for adsorption and removal of Pb(II) from aqueous solutions. J Iran Chem Soc. 2012;9:373-382. https://doi.org/10.1007/s13738-011-0047-2
10. Godwin J, Abdus-Salam N, Adegoke IH, Njimou JR, Akor EJ, Etong ID, et al. Two step fabrication of nano-ZnO-α-FeOOH composite for experimental and modeling studies of removal of indigo carmine and alizarin red s in batch process. Chem Afr. 2023;6(3):1305-1319. https://doi.org/10.1007/s42250-022-00567-2
11. Godwin J, Njimou JR, Abdus-Salam N, Panda PK, Tripathy BC, Ghosh MK, et al. Nanoscale ZnO-adsorbents carefully designed for the kinetic and thermodynamic studies of Rhodamine B. Inorg Chem Commun. 2022;138:109287. https://doi.org/10.1016/j.inoche.2022.109287
12. Abia AA, Asuquo ED. Lead (II) and Nickel (II) adsorption kinetics from aqueous metal solutions using chemically modified and unmodified agricultural adsorbents. Afr J Biotechnol. 2006;5(16):1475-1482. https://www.ajol.info/index.php/ajb/article/view/43142
13. Foo KY, Hameed BH. Insights into the modeling of adsorption isotherm systems. Chem Eng J. 2010;156(1):2-10. https://doi.org/10.1016/j.cej.2009.09.013
14. Voudrias E, Fytianos K, Bozani E. Sorption–desorption isotherms of dyes from aqueous solutions and wastewaters with different sorbent materials. Global Nest Int J. 2002;4(1):75-83.
15. Temkin MJ, Pyzhev V. Recent modifications to Langmuir isotherms. Acta Physicochim. 1940:217-222.
16. Mohy Eldin MS, Gouda MH, Youssef ME, El-Shazly YM, Farag HA. Removal of methylene blue by amidoxime polyacrylonitrile-grafted cotton fabrics: Kinetic, equilibrium, and simulation studies. Fibers Polym. 2016;17:1884-1897. https://doi.org/10.1007/s12221-016-6373-3
17. El-Ashtoukhy ES, Amin NK, Abdelwahab O. Removal of lead (II) and copper (II) from aqueous solution using pomegranate peel as a new adsorbent. Desalination. 2008;223(1-3):162-173. https://doi.org/10.1016/j.desal.2007.01.206
18. Abechi SE, Gimba CE, Uzairu A, Dallatu YA. Preparation and characterization of activated carbon from palm kernel shell by chemical activation. Res J Chem Sci. 2013;3(7):54-61. https://www.isca.in/rjcs/Archives/v3/i7/8.ISCA-RJCS-2013-095.pdf
19. Dina DJ, Ntieche A, Ndi J, Ketcha Mbadcam J. Adsorption of acetic acid onto activated carbons obtained from maize cobs by chemical activation with zinc chloride (ZnCl2). Res J Chem Sci. 2012;2(9):42-49.
20. Sugumaran P, Susan VP, Ravichandran P, Seshadri S. Production and characterization of activated carbon from banana empty fruit bunch and Delonix regia fruit pod. J Sustain Energy Environ. 2012;3(3):125-132.
21. Ioannidou O, Zabaniotou A. Agricultural residues as precursor for activated carbon production: a review. Renew Sustain Energy Rev. 2007;11:1966-2005.
22. Abdus-Salam N, Buhari M. adsorption of alizarin and fluorescein dyes on adsorbent prepared from mango seed. Pac J Sci Technol.

https://doi.org/10.61577/scpnmia.2024.100005

2014;15(1):232-244.
23. Nassar NN, Ringsred A. Rapid adsorption of methylene blue from aqueous solution by goethite nano-adsorbents. Environ Eng Sci. 2011;29(8):790-797. https://doi.org/10.1089/ees.2011.0263
24. Ma Y, Wang SG, Fan M, Gong WX, Gao BY. Characteristics and defluoridation performance of granular activated carbons coated with manganese oxides. J hazard mater. 2009;168(2-3):1140-1146. https://doi.org/10.1016/j.jhazmat.2009.02.145
25. Awwad AM, Salem NM. A green and facile approach for synthesis of magnetite nanoparticles. Nanosci Nanotechnol J. 2012;2(6):208-213. http://dx.doi.org/10.5923/j.nn.201206.09
26. Hou Y, Yu J, Gao S. Solvothermal reduction synthesis and characterization of superparamagnetic magnetite nanoparticle. J Mater Chem. 2003;13(8):1983-1987. https://doi.org/10.1039/B305526D
27. Florido A, Valderrama C, Arévalo JA, Casas I, Martínez M, Miralles N. Application of two sites non-equilibrium sorption model for the removal of Cu (II) onto grape stalk wastes in a fixed-bed column. Chem Eng J. 2010;156(2):298-304. https://doi.org/10.1016/j.cej.2009.10.020
28. Shahryari Z, Goharrizi AS, Azadi M. Experimental study of methylene blue adsorption from aqueous solutions onto carbon nano-tubes. Int J Water Res Environ Eng. 2010;2(2):16-28.
29. Rao MM, Ramana DK, Seshaiah K, Wang MC, Chien SC. Removal of some metal ions by activated carbon prepared from Phaseolus aureus hulls. J hazard Mater. 2009;166(2):1006-1013. https://doi.org/10.1016/j.jhazmat.2008.12.002
30. Hashem FS. Adsorption of methylene blue from aqueous solutions using Fe3O4 /bentonite nanocomposite. Hazard Mater. 2012;133:203-211.
31. Rattanaphani S, Chairat M, Bremner JB, Rattanaphani V. An adsorption and thermodynamic study of lac dyeing on cotton pretreated with chitosan. Dyes Pigments. 2007;72(1):88-96. https://doi.org/10.1016/j.dyepig.2005.08.002
32. Garg VK, Amita M, Kumar R, Gupta R. Basic dye (methylene blue) removal from simulated wastewater by adsorption using indian rosewood sawdust: a timber industry waste. Dyes Pigments. 2004;63(3):243 -250. https://doi.org/10.1016/j.dyepig.2004.03.005
33. Pekkuz H, Uzun İ, Güzel F. Kinetics and thermodynamics of the adsorption of some dyestuffs from aqueous solution by popular sawdust. Bioresour Technol. 2008;99(6):2009-2017. https://doi.org/10.1016/j.biortech.2007.03.014
34. Dutta S, Bhattacharyya A, Ganguly A, Gupta S, Basu S. Application of response surface methodology for preparation of low-cost adsorbent from citrus fruit peel and for removal of methylene blue. Desalination. 2011;275(1-3):26-36. https://doi.org/10.1016/j.desal.2011.02.057
35. Ncibi MC, Mahjoub B, Seffen M. Kinetic and equilibrium studies of methylene blue biosorption by Posidonia oceanic (L) fibres. J Hazard Mater. 2007;139(2):280-285. https://doi.org/10.1016/j.jhazmat.2006.06.029
36. Tsai WT, Chen HR, Kuo KC, Lai CY, Su TC, Chang YM, et al. The adsorption of methylene blue from aqueous solution using waste aquacultural shell powder. Environ Eng Manag J. 2009;19(3):165-172.
37. Alzaydien AS. Adsorption of methylene blue from aqueous solution onto a low-cost natural Jordanian Tripoli. Am J Appl Sci. 2009;6(6):1047-1058.
38. Elmorsi TM. Equilibrium isotherms and kinetics studies of removal of methylene blue dye by adsorption onto miswak leaves as a natural adsorbent. J Environ Prot. 2011;2:817-827. http://dx.doi.org/10.4236/jep.2011.26093
39. Eman A, Ashour MAT, Patrick JP. Use of agricultural-based waste for basic dye sorption from aqueous solution: kinetics and isotherm studies. Am J Chem Eng. 2014;2(6):92-98. http://dx.doi.org/10.11648/j.ajche.20140206.14
40. Gupta VK, Mohan D, Sharma S, Sharma M. Removal of basic dyes (rhodamine B and methylene blue) from aqueous solution using bagasse fly ash. Sep Sci Technol. 2000;35(13):2097-2113. https://doi.org/10.1081/SS-100102091
41. Safa Y, Bhatti HN. Adsorptive removal of direct dyes by low-cost rice husk: effect of treatments and modifications. Afr J Biotechnol. 2011;10(16):3128-3142. https://doi.org/10.5897/AJB10.1302
42. Li Y, Du Q, Liu T, Peng X, Wang J, Sun J, et al. Comparative study of methylene blue dye adsorption onto activated carbon, graphene oxide, and carbon nanotubes. Chem Eng Res Des. 2013;91(2):361-368. https://doi.org/10.1016/j.cherd.2012.07.007
43. Sampranpiboon P, Feng X. Kinetic model of Cr (VI) adsorption onto carbonized oil palm kernel with potassium hydroxide activation. Int J Adv Chem Eng Biol Sci. 2016;3(1):66-71. https://iicbe.org/upload/2373U0416211.pdf
44. Idris S, Ndamitso MM, Iyaka YA, Muhammad EB. Sawdust as adsorbent for the removal of methylene blue from aqueous solution: adsorption and equilibrium studies. J Chem Eng. 2012;1(1):11-24.
45. Amrhar O, Nassali H, Elyoubi MS. Adsorption of a cationic dye methylene blue onto Moroccan illitic clay. J Mater Environ Sci. 2015;6(11):3054-3065.

https://doi.org/10.61577/scpnmia.2024.100005